The Physics of Space Plasmas

Dynamics of the Equatorial Ionosphere

William J. Burke
19 December 2012
University of Massachusetts, Lowell

BOSTON COLLEGE
ISR
INSTITUTE FOR SCIENTIFIC RESEARCH

Lecture 11

- **Equatorial Spread-F**
  - **Phase-screen transmission model**
  - **Rayleigh-Taylor approximation**
  - **Equatorial plasma bubbles**
  - **Generalized Rayleigh-Taylor modeling at NRL**
- **Ripple effects of Gulf War I**
  - **The Communications Navigation Outage Forecast System (C/NOFS)**
  - **Preparing for C/NOFS: Mission definition - DMSP Initiative**
  - **Global season-longitude climatologies**
  - **Pre-reversal electric fields in quiet and storm times**
- **C/NOFS launch April 2008: A new world revealed**
  - **Ground – space connections**

Equatorial Ionospheric Dynamics

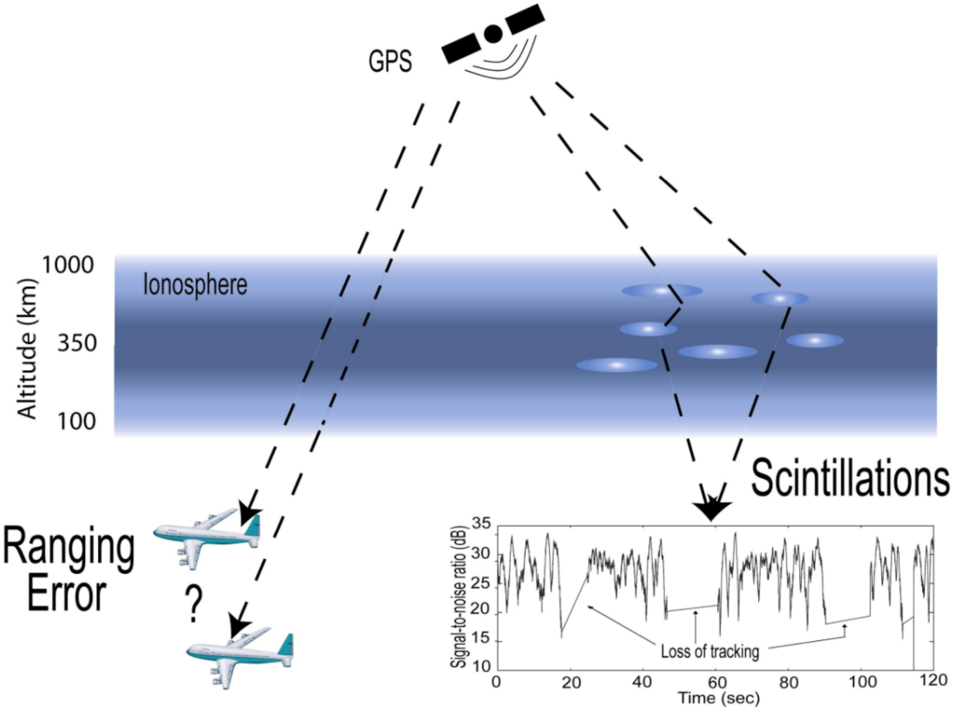

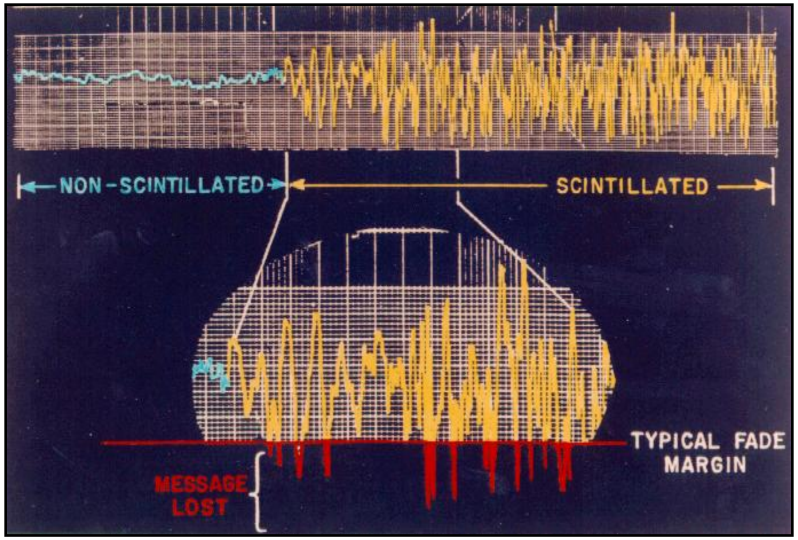

- **<u>Ranging errors</u>: need good electron density profile (EDP) model**

- **Sever scintillations occur at polar and equatorial magnetic latitudes but for very different reasons.**

Rufenach, C. L. (1975), Ionospheric scintillation by a random phase screen: Spectral approach, *Radio Sci, 10*, 155-165.

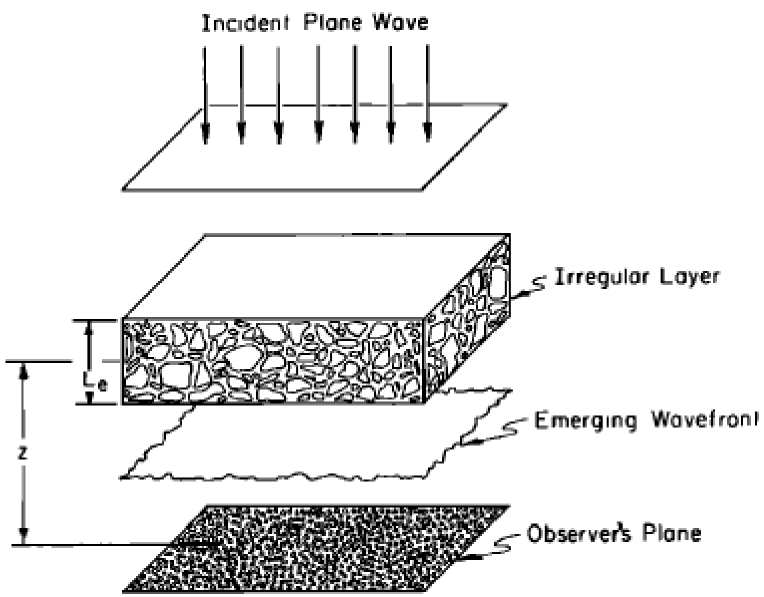

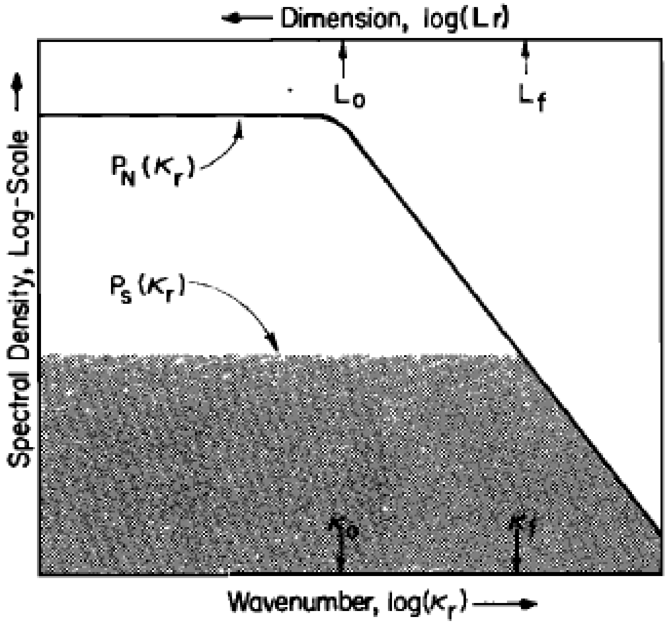

$$\text{Fresnel length} = \sqrt{2\lambda z}$$

$$S_4 = \sigma / \overline{I}$$

<u>Equation for Fresnel length</u>

- **λ, the wavelength (1.2 meters), is equal to the speed of light divided by signal frequency; z is the altitude of the F-layer peak.**
- **There must be high spectral power at the ~1 km Fresnel length to produce 250 MHz scintillation**

Equatorial Ionospheric Dynamics

Balsley et al., Equatorial Spread F: Recent observations and a new interpretation, *J. Geophys. Res., 77*, 5625 – 5628, 1972.

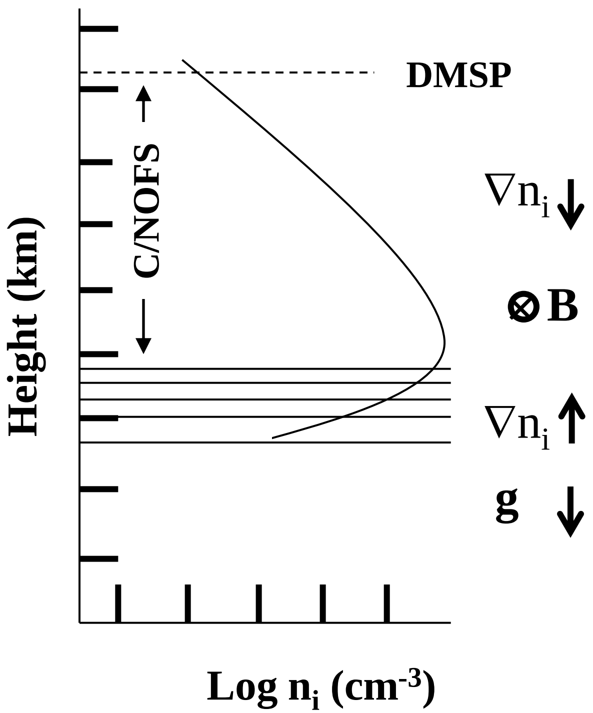

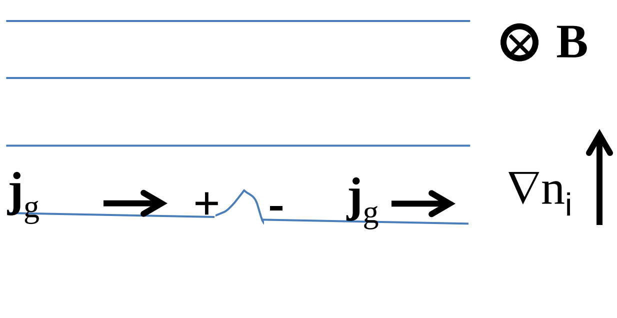

$\mathbf{v}_g = m_i\,(\mathbf{g} \times \mathbf{B}) / q\mathbf{B}^2$

$\mathbf{j}_g = n_i\, q\, \mathbf{v}_g$

$\mathbf{j}_g = n_i m_i\,(\mathbf{g} \times \mathbf{B}) / \mathbf{B}^2$

$\mathbf{j}_g = (n_i - \delta n_i) m_i\,(\mathbf{g} \times \mathbf{B}) / \mathbf{B}^2 + \sigma_P\, \delta \mathbf{E}_A$

$\delta E_A = (q\, g / \Omega_i)\,(\delta n_i / \sigma_P)$

$V_E = \delta E_A / B$ upwards if $\delta \mathbf{E}_A$ eastwards

$\sigma_P = (n\, q / B)\,(\nu_{in} / \Omega_i)$

$V_E = \delta E_A / B$ upwards if $\delta \mathbf{E}_A$ eastwards

δn_i grows if ∇n_i is upwards with a growth rate

$\gamma = -(\mathbf{g} / \nu_{in})\, \nabla \log n_i$

Equatorial Ionospheric Dynamics

Woodman and La Hoz, Radar observations of F region equatorial irregularities*, J. Geophys. Res., 81*, 5447 – 5466, 1976.

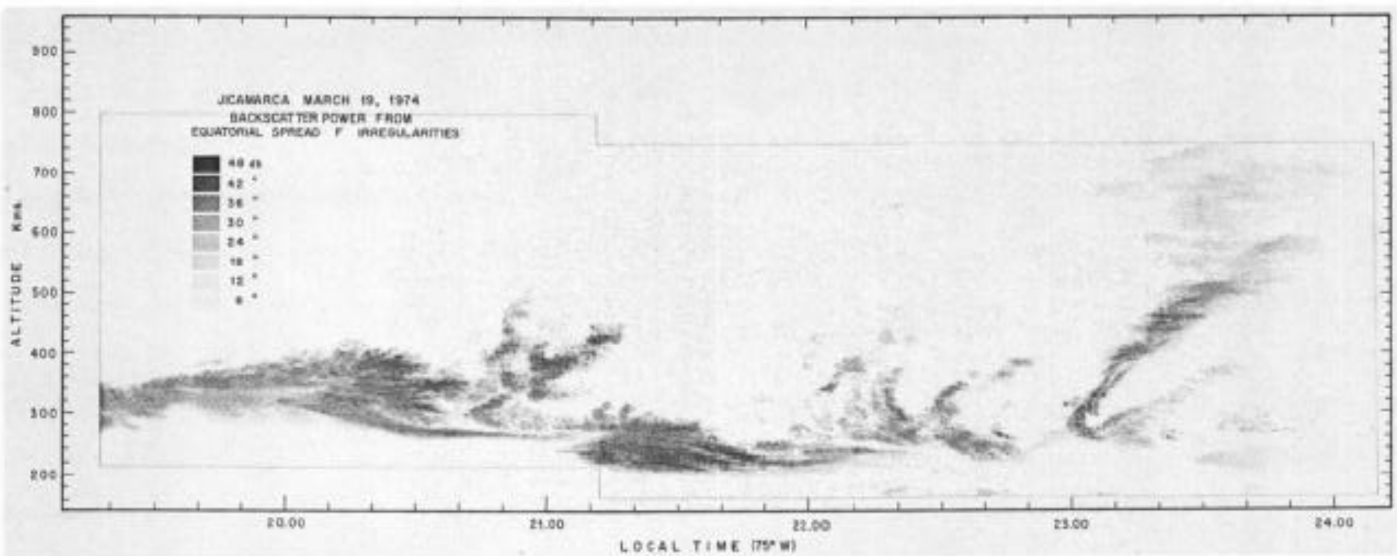

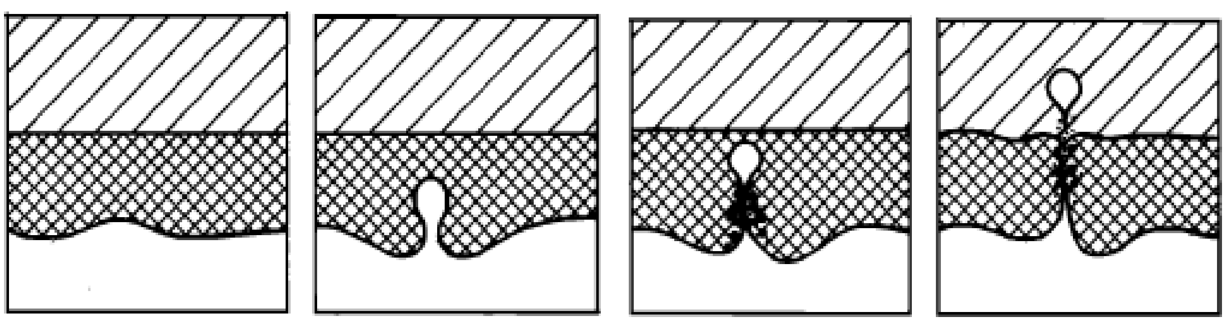

Equatorial Ionospheric Dynamics

Ott, E., Theory of Rayleigh-Taylor bubbles in the equatorial ionosphere, *J. Geophys. Res. 83*, 2066 – 2070, 1978.

- Showed that if $\mathbf{E} = \mathbf{E}_0 + \delta\mathbf{E}$ and we transform into a coordinate systems moving with a velocity $\mathbf{V}_E = (\mathbf{E}_0 \times \mathbf{B}) / \mathbf{B}^2$ then we can define a parameter $\mathbf{g}' = \mathbf{g} - \nu_{in}\ \mathbf{V}_E$.

- The growth rate for this generalized Rayleigh-Taylor instability becomes

$$\gamma = -(g' / \nu_{in})\ \nabla \log n_i$$

- Showed that in the non-linear limit irregularities can grow into bubbles that penetrate into the topside ionosphere.

- In the now most famous unpublished paper in the history of ionospheric physics *Haerendel* argued that the R-T instability is no local, but involves entire flux tubes and that we must use Σ rather than σ in calculating growth rates.

Haerendel, G., Theory of equatorial spread F, Max-Planck-Institut für Physik und Astrophysik, Munich, 1974.

Equatorial Ionospheric Dynamics

NRL Simulations

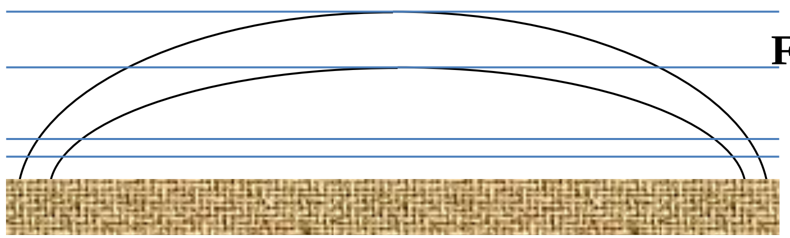

Growth Rate **Electric Field** **Neutral Wind** **Gravity**

$$\gamma \approx \frac{\sum_F}{\sum_F + \sum_E}\left[\frac{\boldsymbol{E}\times\boldsymbol{B}}{B^2} + U_n + \frac{g}{\nu^{eff}}\right]\frac{1}{N}\frac{\partial N}{\partial h}$$

Conductance **Magnetic Field** **Log Density Gradient**

Scannapieco, A. J., and S. L. Ossakow (1976), Nonlinear equatorial spread F, *Geophys. Res. Lett., 3, 451-454.*

R-T growth controlled by the variability of

E, U_n, Σ_E, Σ_F, ν^{eff}

and, through flux-tube integrated quantities,

by the F-layer's height.

Equatorial Ionospheric Dynamics

Schematic of Sq current system near 12:00 UT

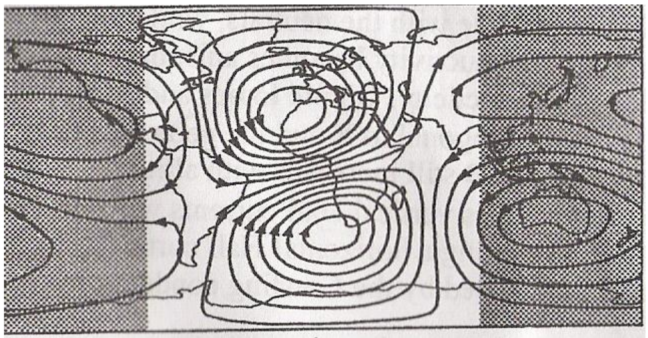

ROCSAT measurements of vertical plasma drifts: season - longitude

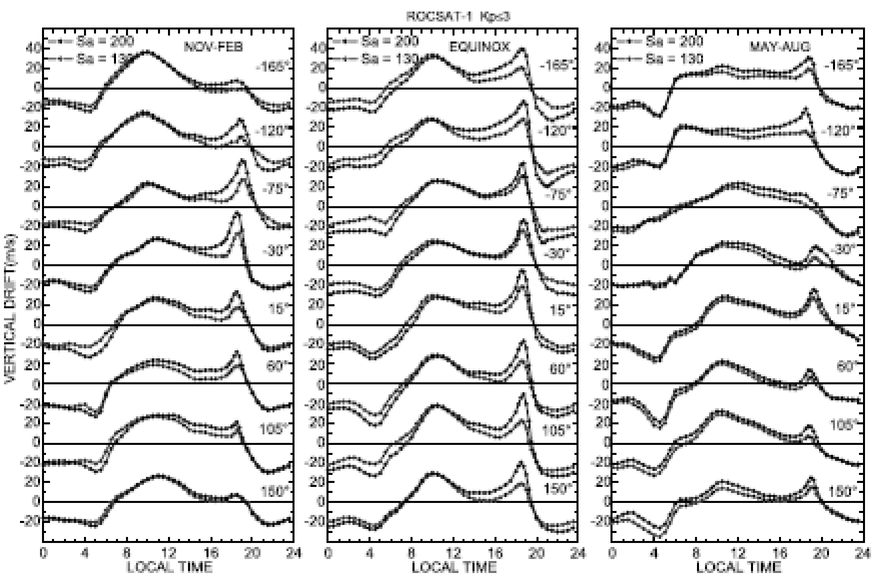

Pre-reversal enhancement signatures observed with Jicamarca ISR

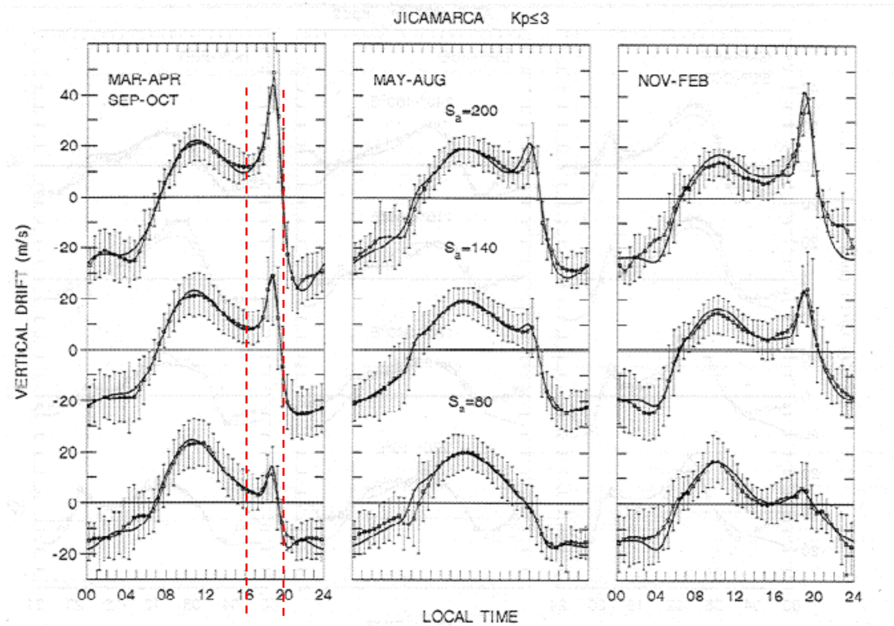

Scherliess, L., and B. G. Fejer (1997), Storm time dependence of equatorial disturbance dynamo zonal electric fields, *J. Geophys. Res., 102*, 24,037.

Fejer, B. G., J. W. Jansen and S.-Y. Su (2008), Quiet time equatorial F region vertical plasma drift model drifts derived from ROCSAT-1 observations. *J. Geophys. Res., 113*, A05304.

Equatorial Ionospheric Dynamics

In responses to challenges revealed during of Gulf war AFRL instituted a 4-pronged C/NOS program

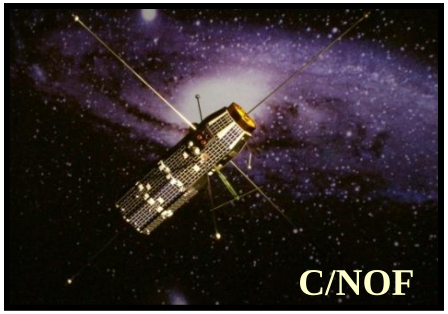

- **C/NOFS Satellite to fly in 13° inclined orbit**

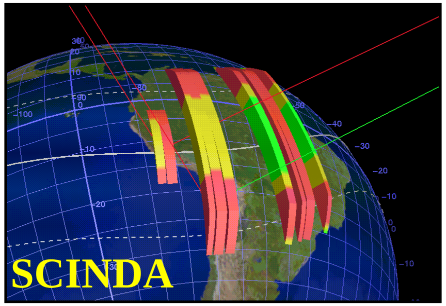

- **Ground bases SCINDA network**
- **Computer modeling of equatorial ionosphere**
- **Utilize existing resources**

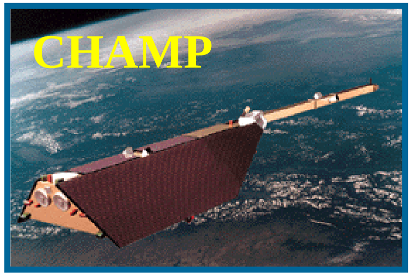

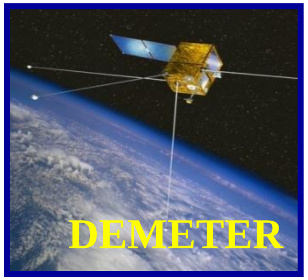

Equatorial Ionospheric Dynamics

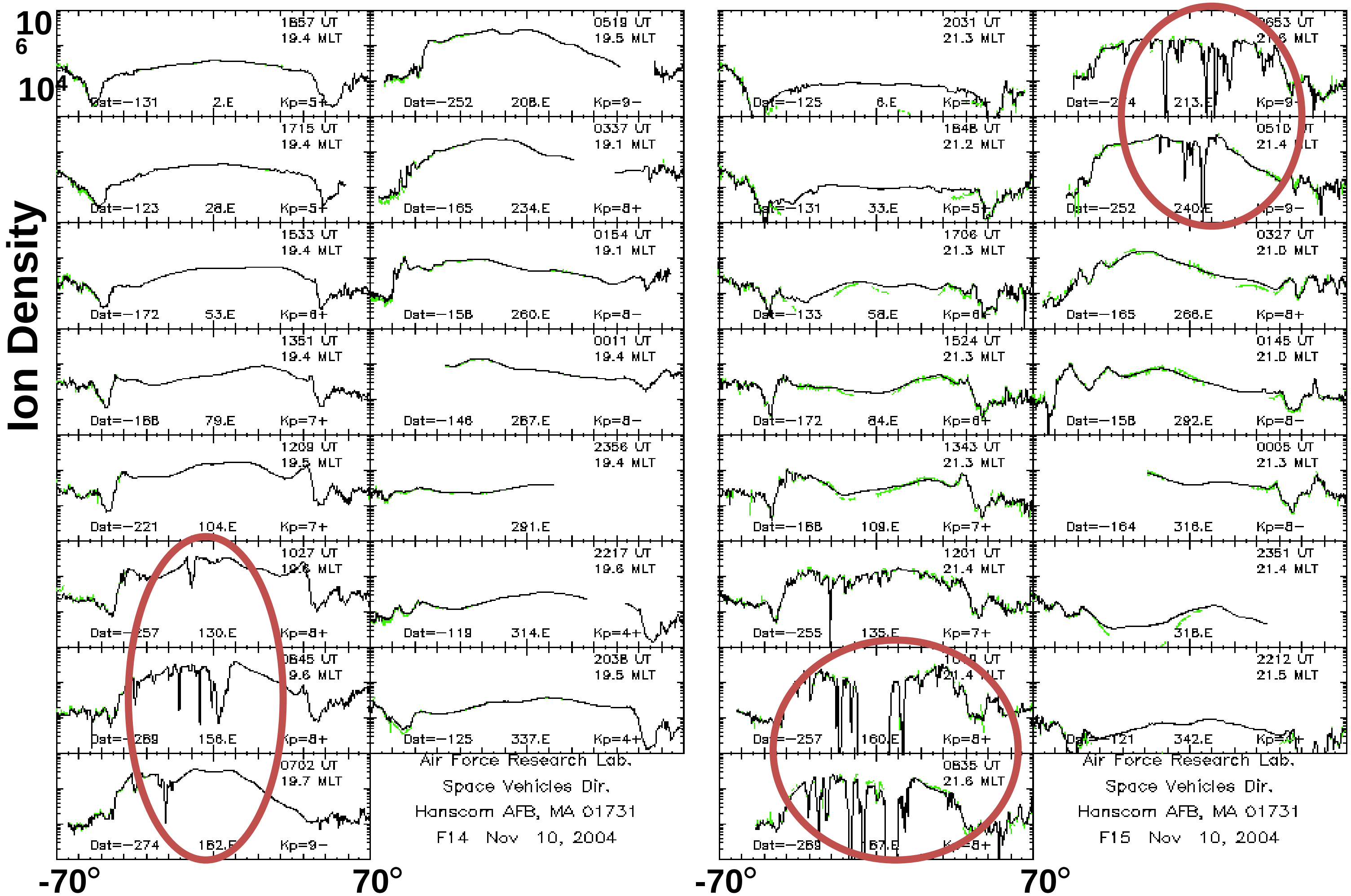

Fejer, B. G., J. W. Jensen, T. Kikuchi, M. A. Abdu, and J. L. Chau (2007), Equatorial ionospheric electric fields during the November 2004 magnetic storm, *J. Geophys. Res.*, *112*, A10304, doi:10.1029/2007JA012376.

Equatorial Ionospheric Dynamics

DMSP EPB Database 1989 - 2006

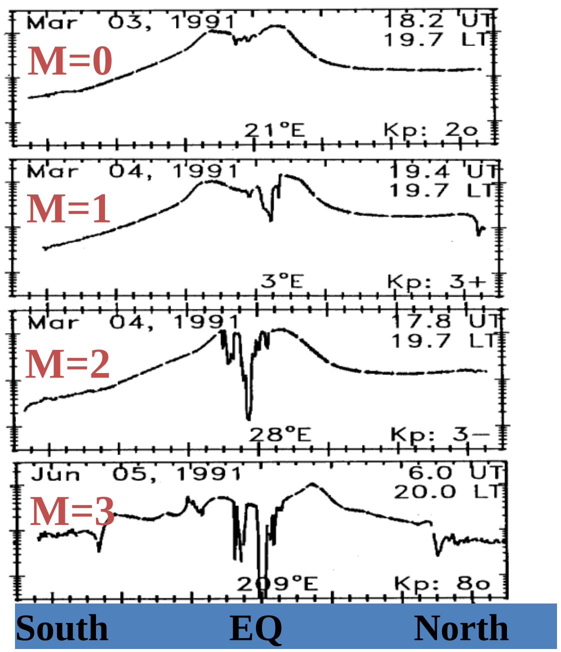

M-0 if dN ≤ 2
M-1 if 2 < dN ≤ 10
M-2 if 10 < dN ≤ 100
M-3 if dN > 100

Year	Spacecraft	LT (Hr)	Orbits	EPBs	M-0	M-1	M-2	M-3
1989	F09	21	5121	1109	297	762	50	0
1990	F09	20.9	5091	1089	289	735	62	3
1991	F09	20.7	5040	1024	304	664	55	1
1991	F10	20	4925	675	218	351	86	20
1992	F10	20.7	5043	755	306	406	41	2
1993	F10	21.3	5092	389	186	191	11	1
1994	F10	21.7	3749	121	53	58	10	0
1994	F12	21.4	1575	42	33	8	1	0
1995	F12	21.4	4976	130	51	71	8	0
1996	F12	21.5	5122	73	35	36	2	0
1997	F12	21.4	3343	47	24	23	0	0
1997	F14	20.6	3104	51	18	32	1	0
1998	F12	21.2	4123	283	106	169	7	1
1998	F14	20.7	4993	275	129	138	8	0
1999	F12	20.8	4290	431	83	330	13	5
1999	F14	20.8	4839	460	167	285	6	2
2000	F12	20.3	4556	637	85	509	41	2
2000	F14	20.7	4969	821	298	493	26	4
2000	F15	21.3	5060	1034	377	620	30	7
2001	F12	19.8	4557	404	60	305	34	5
2001	F14	20.6	4787	861	174	643	38	6
2001	F15	21.5	5095	1014	292	699	20	3
2002	F14	20.3	4889	781	160	563	55	3
2002	F15	21.5	5113	991	279	672	40	0
2003	F14	19.9	4732	156	37	108	5	6
2003	F15	21.4	5149	385	84	275	15	11
2004	F14	19.6	4777	30	10	14	6	0
2004	F15	21.3	5123	267	63	180	14	10
2004	F16	19.9	5131	77	18	51	7	1
2005	F15	20.8	5139	140	56	68	13	3
2005	F16	20.2	5143	64	27	32	5	0
2006	F15	20.3	5130	51	26	25	0	0
2006	F16	20.2	5122	35	21	13	1	0
Totals			154898	14702	4366	9529	711	96

Equatorial Ionospheric Dynamics

Physics-based Model: Dynamics of Equatorial Plasma Bubbles

PBMOD 3-D images of evolving plasma bubbles
by altitude and longitude (left), altitude and latitude (right)

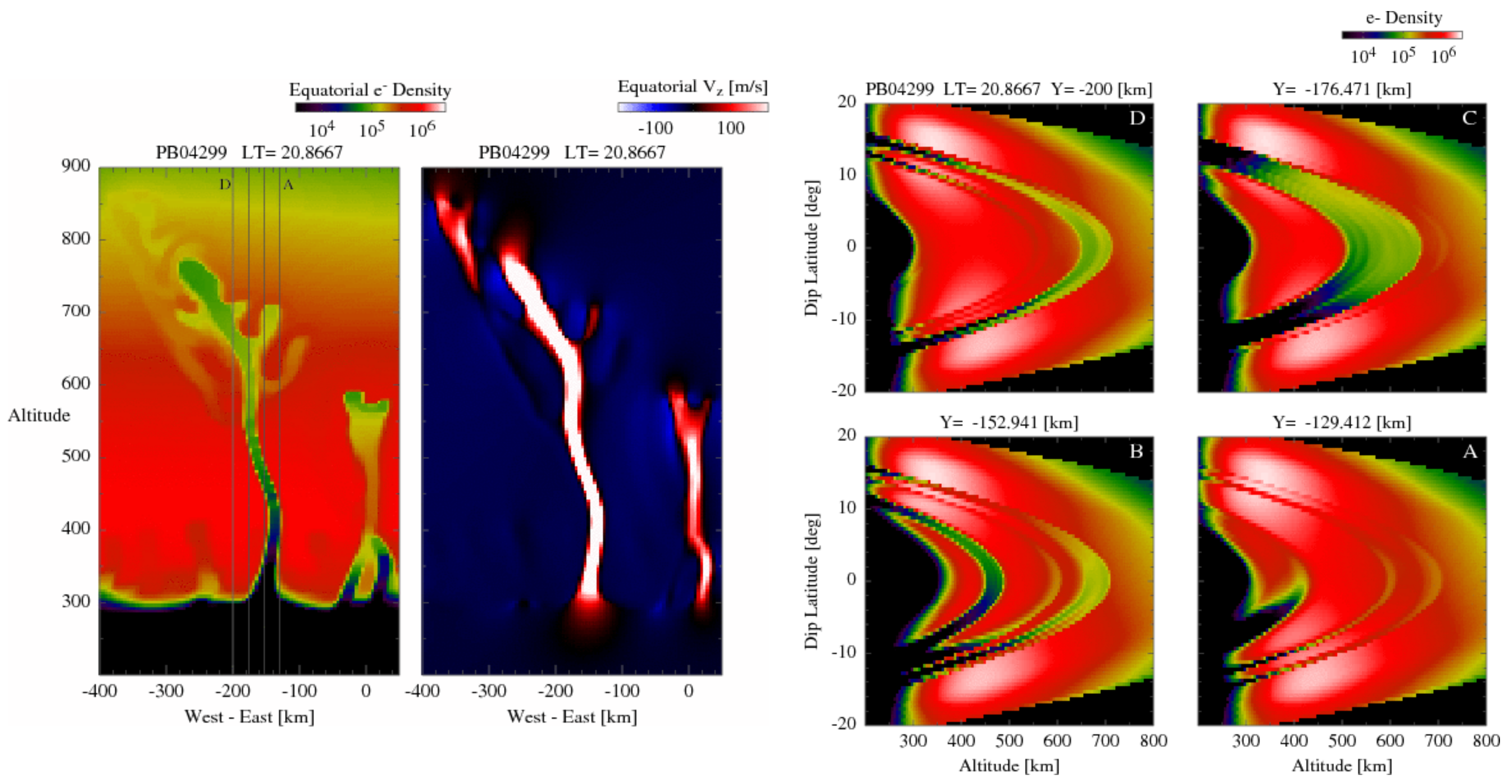

C/NOFS observations on successive orbits of sustained plasma depletion regions support new PBMOD 3-D model development

Equatorial Ionospheric Dynamics

Optical Signatures of Equatorial Plasma Bubbles

- In the mid 1980s Ed Weber of AFGL conducted a campaign in Brazil to look for EPB signatures in 6300 Å airglow. $O^{+} + e^{-} \rightarrow O + h\nu$
- Identified long black streaks as a lack of O+ ions that could recombine and emit photons.
- The GUVI and SSUSI sensors on TIMED and DMPS measure 1356 Å emissions, also a recombination line.
- Developed tomographic techniques to make 3D images of EPBs

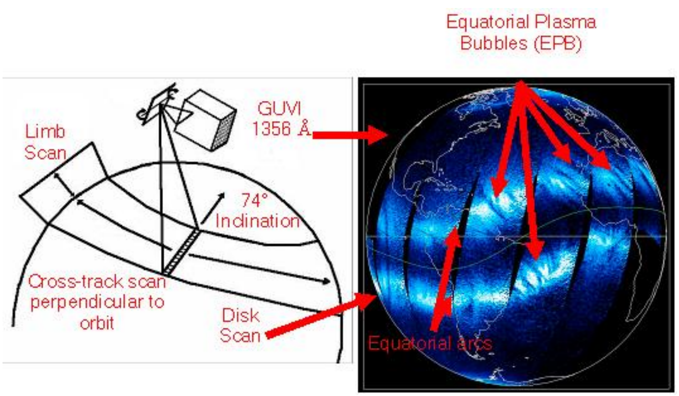

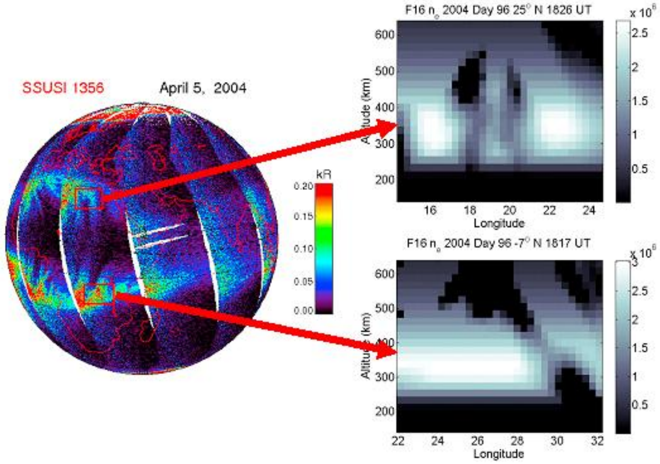

Comberiate, J., and L. J. Paxton (2010), Coordinated UV imaging of equatorial plasma bubbles using TIMED/GUVI and DMSP/SSUSI, *Space Weather, 8*, S10002.

Equatorial Ionospheric Dynamics

Reflecting on a season-longitude variations of scintillation occurrence and R-T growth rates

$$\gamma \approx \frac{\sum_F}{\sum_F + \sum_E}\left[\frac{\boldsymbol{E}\times\boldsymbol{B}}{B^2} + U_n + \frac{g}{\nu^{eff}}\right]\frac{1}{N}\frac{\partial N}{\partial h}$$

Roland Tsunoda suggested that rates should be high at the times of year when both ends of flux tube went into darkness simultaneously.

- **The terminator line has a tilt angle Ψ = 23.5 Sin[(day - ϕ) / 365]**
- **Compare DMSP EPB rates versus time/places where Ψ = declination.**

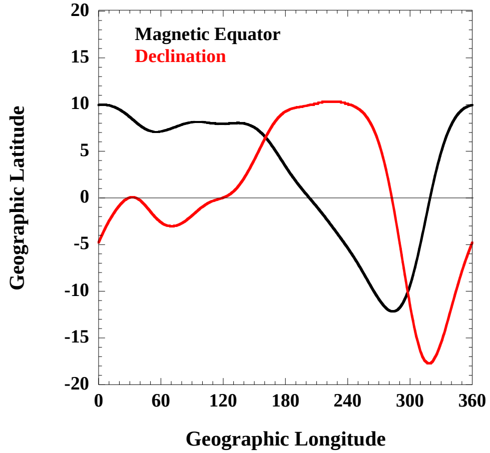

Tsunoda, R. T. (1985), Control of the seasonal and longitudinal occurrence of equatorial scintillations by the longitudinal gradient in the integrated E-region Pedersen conductivity, *J. Geophys. Res.*, *90*, 447.

Equatorial Ionospheric Dynamics

DMSP EPB Season- Longitude Climatology: Solar Maxima

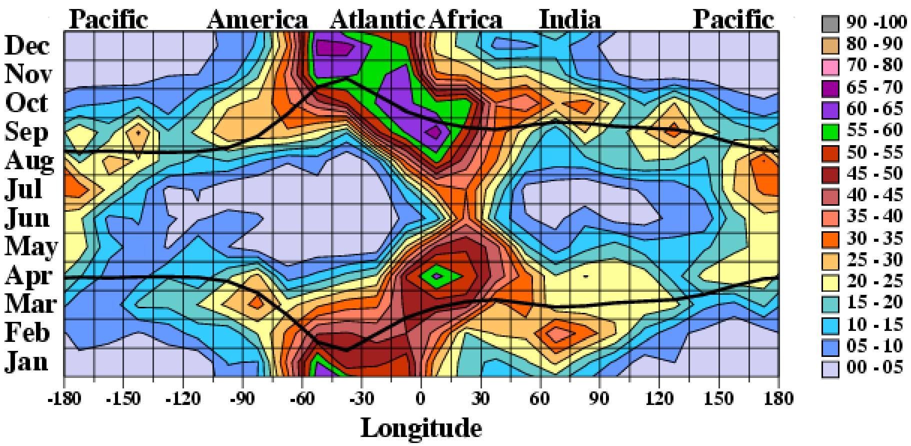

During solar maximum 1989 - 1992, EPBs occurred throughout the year in the Atlantic-Africa sector; rates were highest (60% - 68%) from September to December.

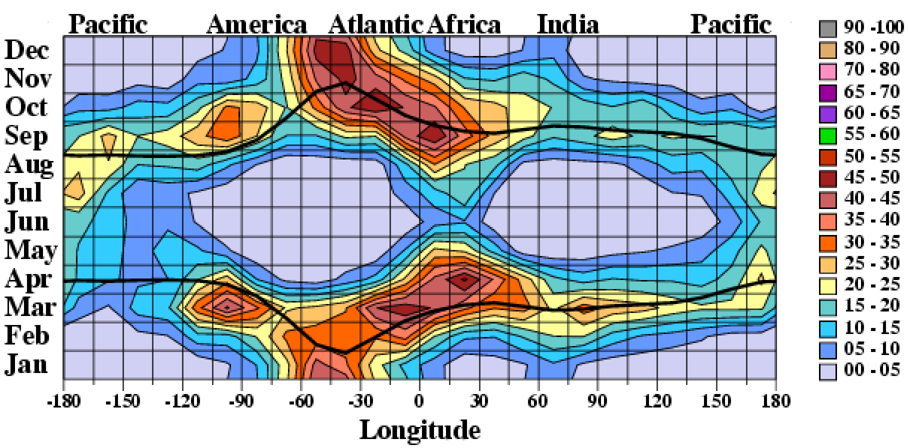

For solar maximum 1999 – 2002, EPB rates were fairly symmetric; high (40% - 51%) in the America-Atlantic-Africa sector both early and late in the year.

Black lines represent two days per year when/where terminator and declination align

DMSP F14 and F15 EPB Rates: 2000 - 2004

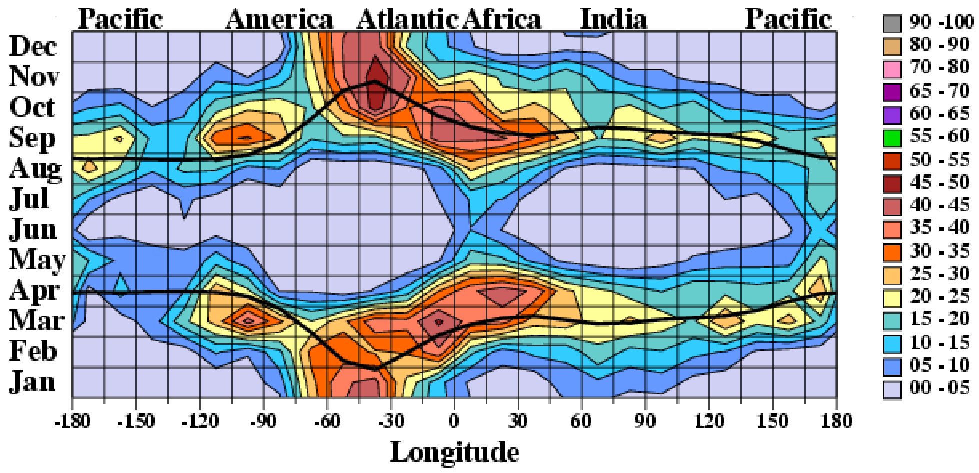

F14
19.6 to 20.7 LT

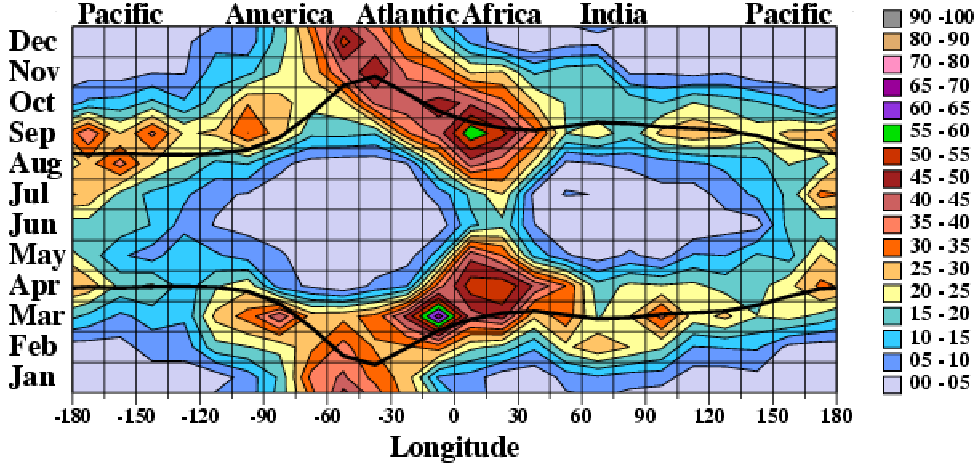

F15
21.3 to 21.5 LT

DMSP EPB Climatology: Solar Maximum and Minimum

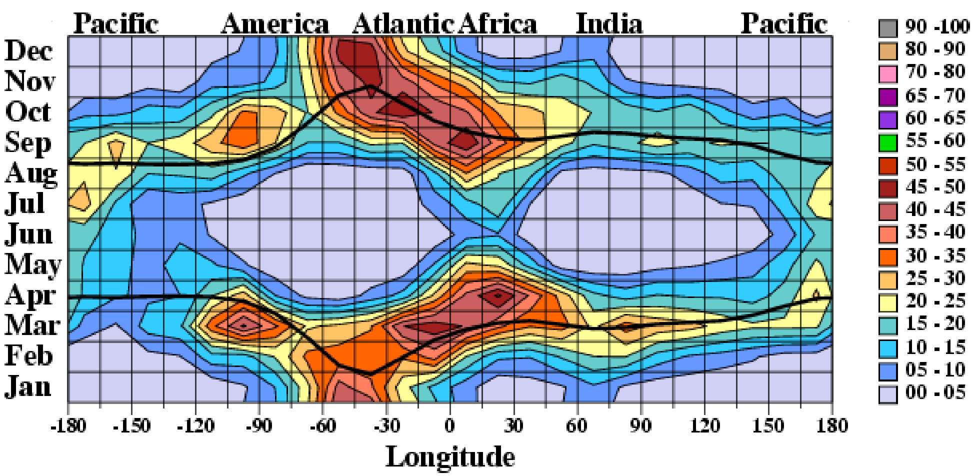

For solar maximum 1999 - 2002, EPB rates were high in America-Atlantic-Africa sector early and late in the year and significantly lower in Pacific sector in November.

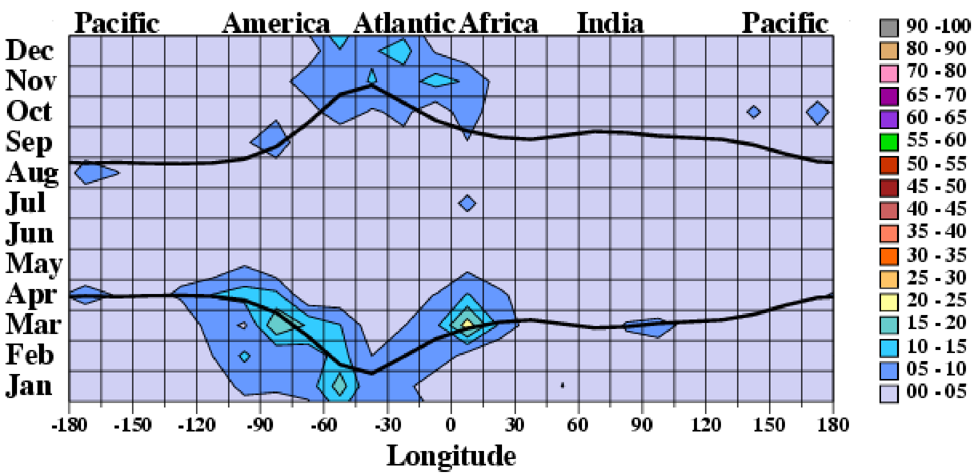

For solar minimum 1994 - 1997, EPB rates were generally < 5% including Pacific sector in November; highest rates (20% - 25%) were in the Atlantic-Africa sector in March.

DMSP EPB Climatology: Solar Maximum and Minimum

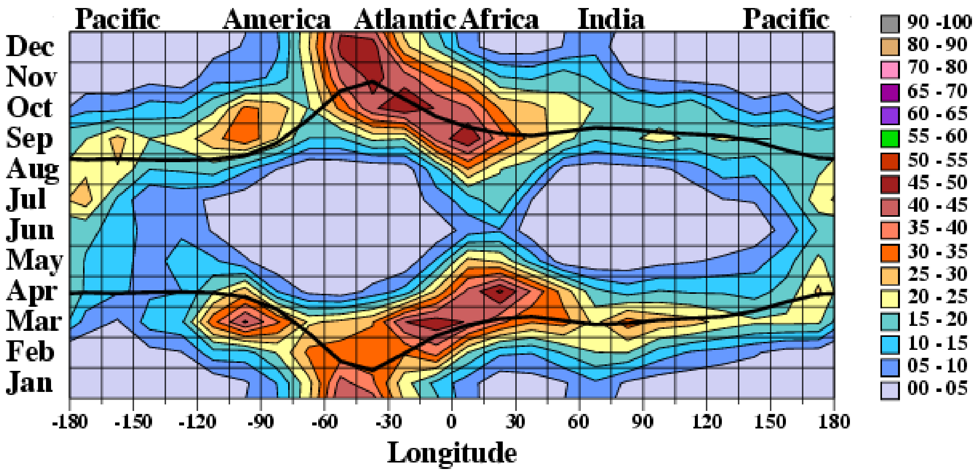

For solar maximum 1999 - 2002, EPB rates were high in America-Atlantic-Africa sector early and late in the year and significantly lower in Pacific sector in November.

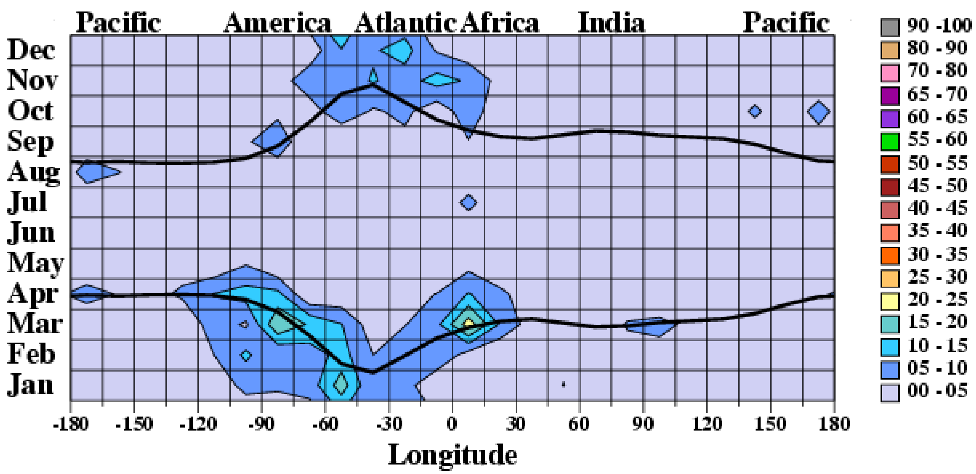

For solar minimum 1994 - 1997, EPB rates were generally < 5% including Pacific sector in November; highest rates (20% - 25%) were in the Atlantic-Africa sector in March.

DMSP EPB Rates: Transition Years 1993 and 1998

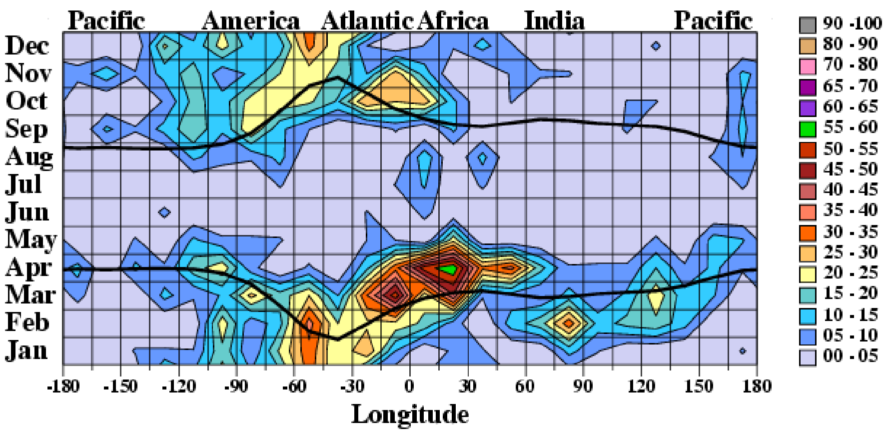

In 1993 as the solar cycle declined, EPB rates were higher in the Atlantic-Africa sector early in the year, from January through April.

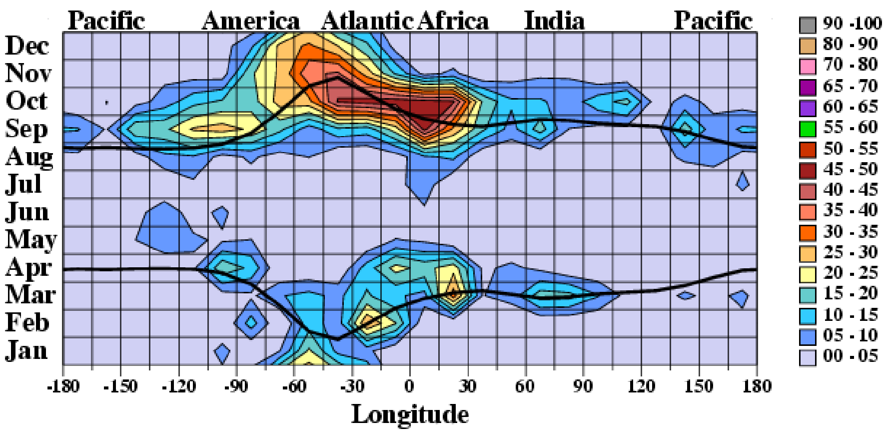

In 1998, as the solar cycle was increasing, EPB rates were higher in the America-Atlantic-Africa sector late in the year, Sept through Nov.

DMSP EPB Climatology: Declining Phase of Solar Cycle

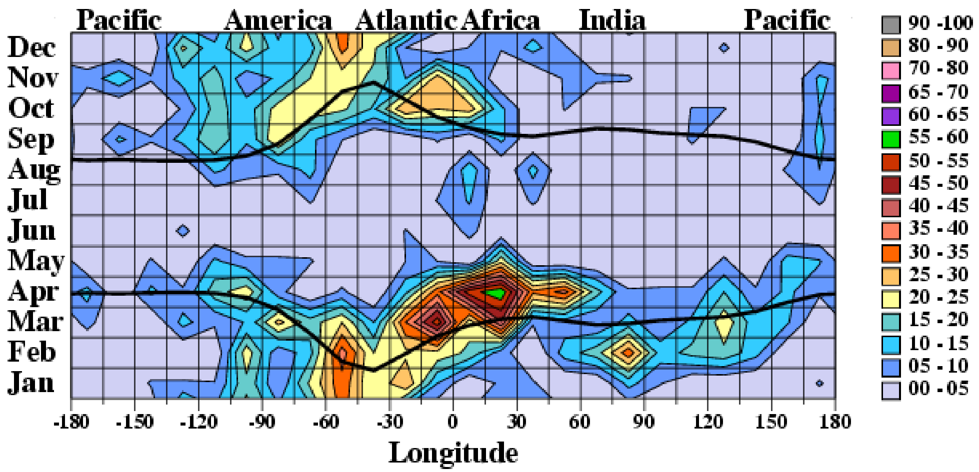

In 1993 as the solar cycle declined, EPB rates were higher in the Atlantic-Africa sector early in the year, from January through April.

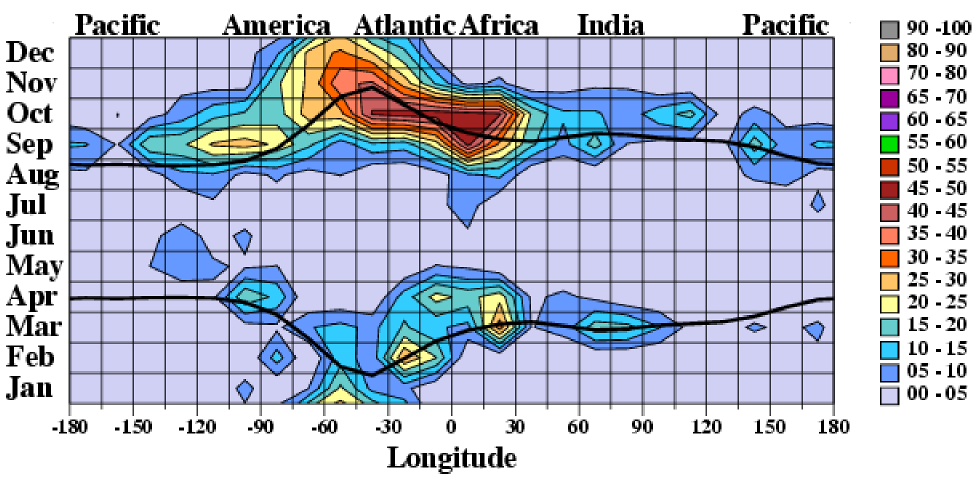

In 1998, as the solar cycle was increasing, EPB rates were higher in the America-Atlantic-Africa sector late in the year, Sept through Nov.

DMSP EPB Climatology: 2004 - 2006

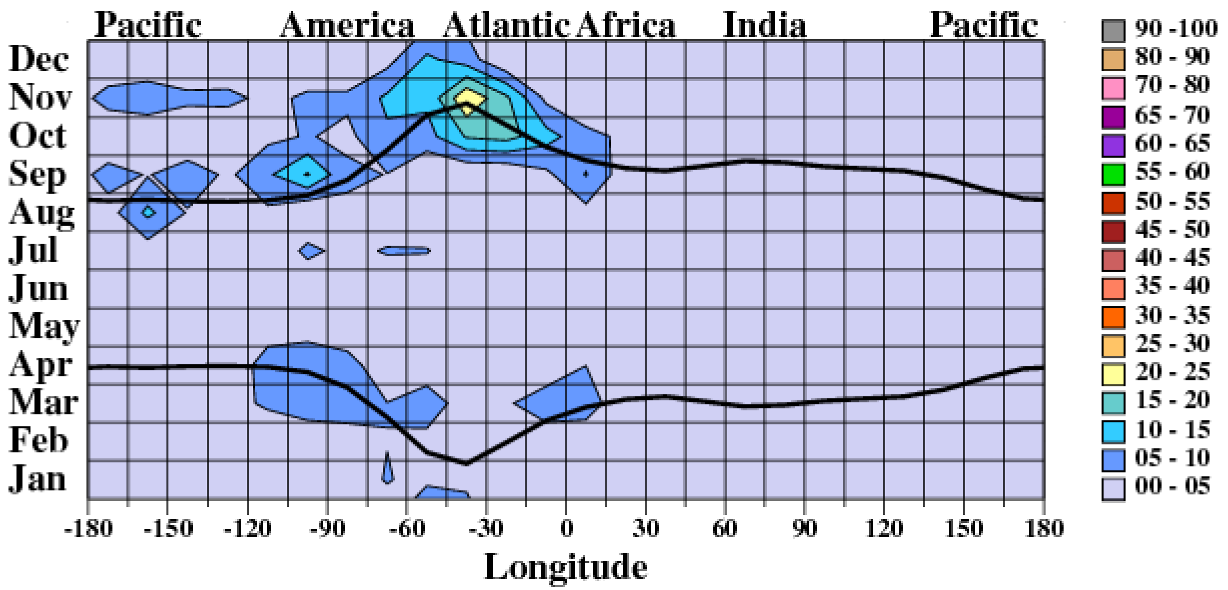

EPB rates were generally extremely low (< 5%) in 2004 – 2006; highest rates (20% – 25%) were observed in the Atlantic during November. There were also several EPBs in the Pacific during the November 2004 storms.

Dawn Depletions: Solar Minimum 2008 – 2009 05:30 LT

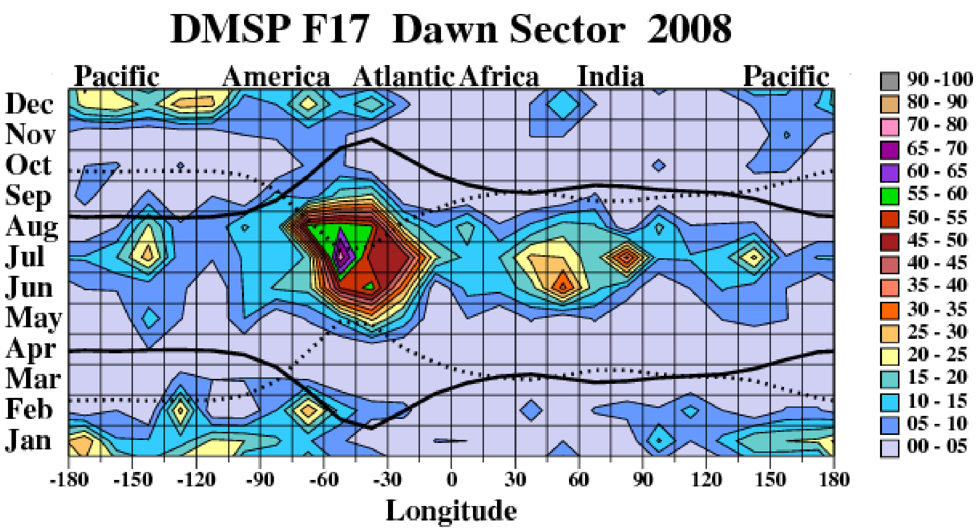

Most dawn topside depletions were observed around the June (Atlantic) and December (Pacific) solstices

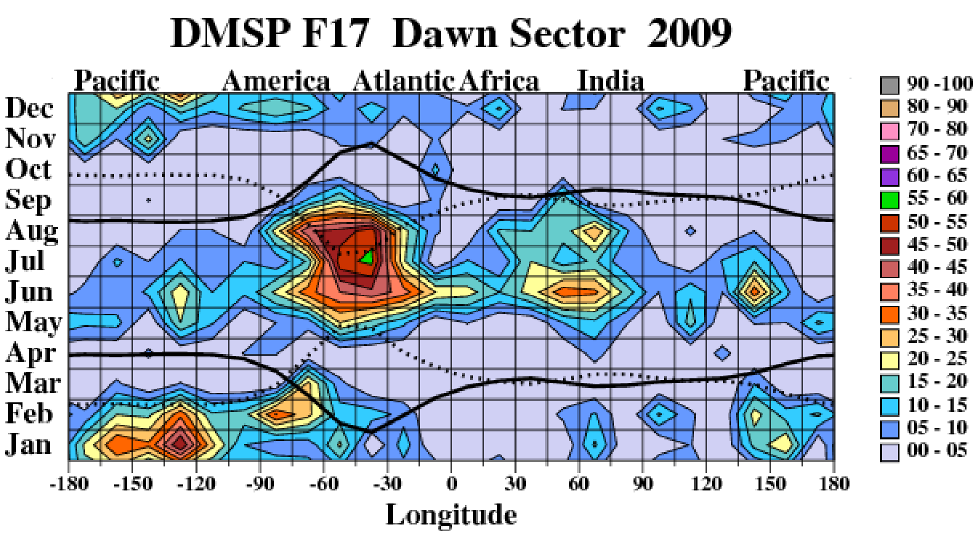

Most dawn topside depletions were observed around the June (Atlantic) and December (Pacific) solstices

Equatorial Ionospheric Dynamics

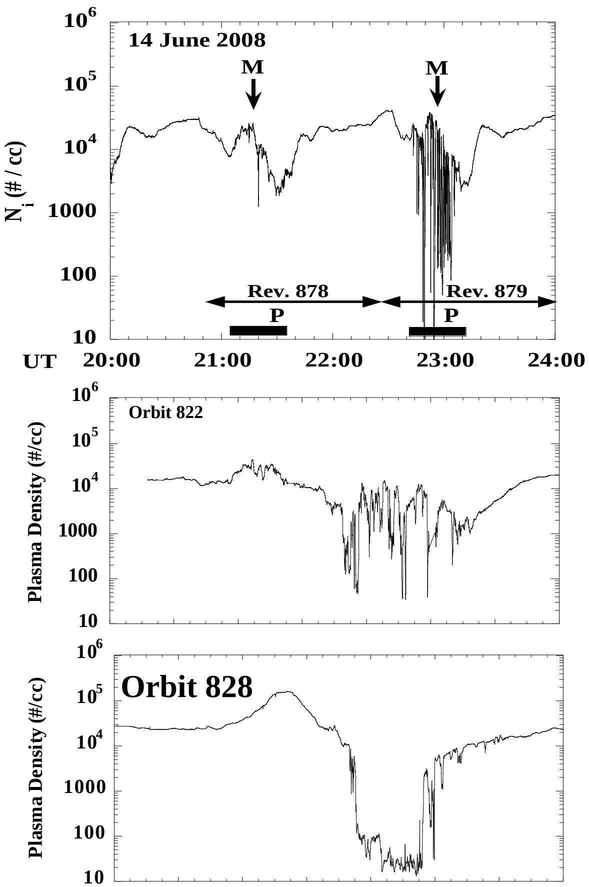

Burke, W J. et al. (2009), C/NOFS observations of plasma density and electric field irregularities at post-midnight local times, *Geophys. Res. Lett.*, *36*, L00C09.

No sign of pre-reversal enhancement

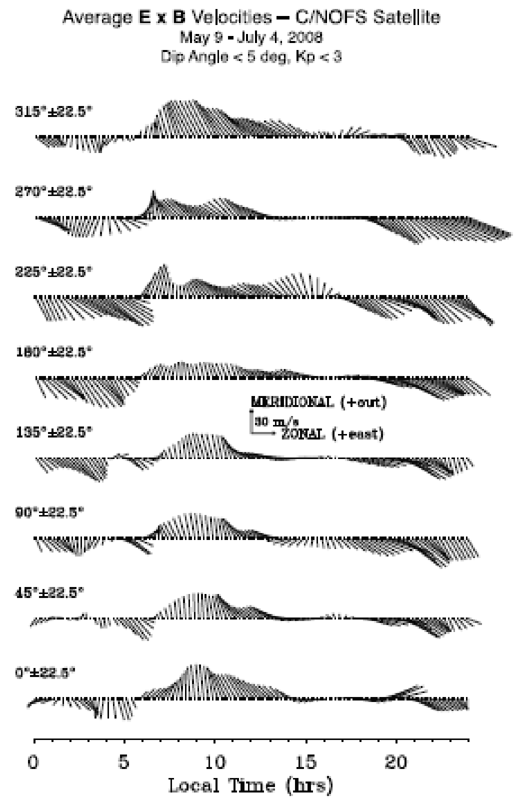

Pfaff, R., et al. (2010), Observations of DC electric fields in the low-latitude ionosphere and their variations with local time, longitude, and plasma density during extreme solar minimum, *J. Geophys. Res.*, *115*, A12324.

C/NOFS and DMSP encountered extended dawn sector plasma depletions

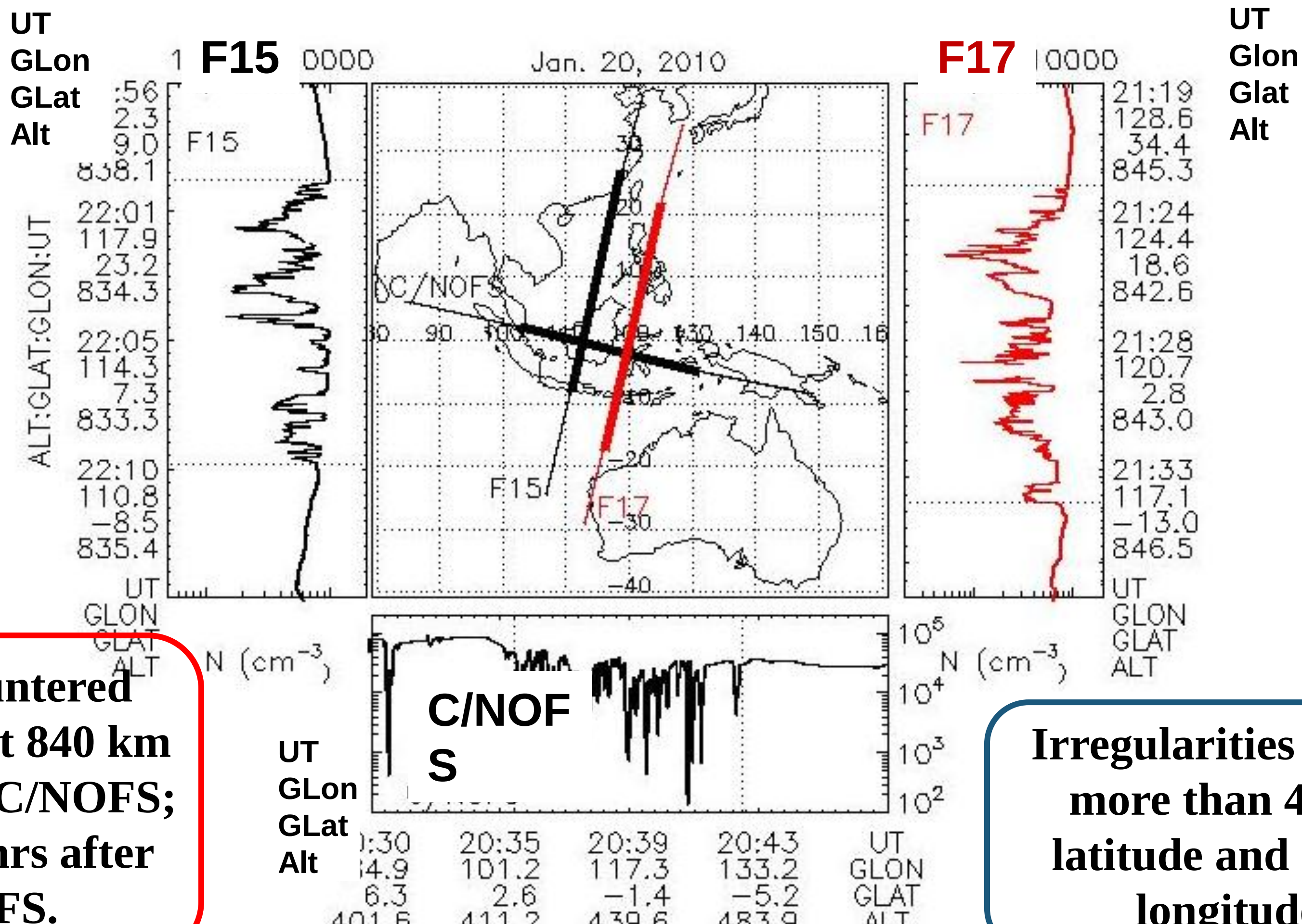

F17 encountered depletions at 840 km ~ 1 hr after C/NOFS; F15 ~ 1.5 hrs after C/NOFS.

Irregularities extend more than 44° in latitude and 30° in longitude.

Equatorial Ionospheric Dynamics

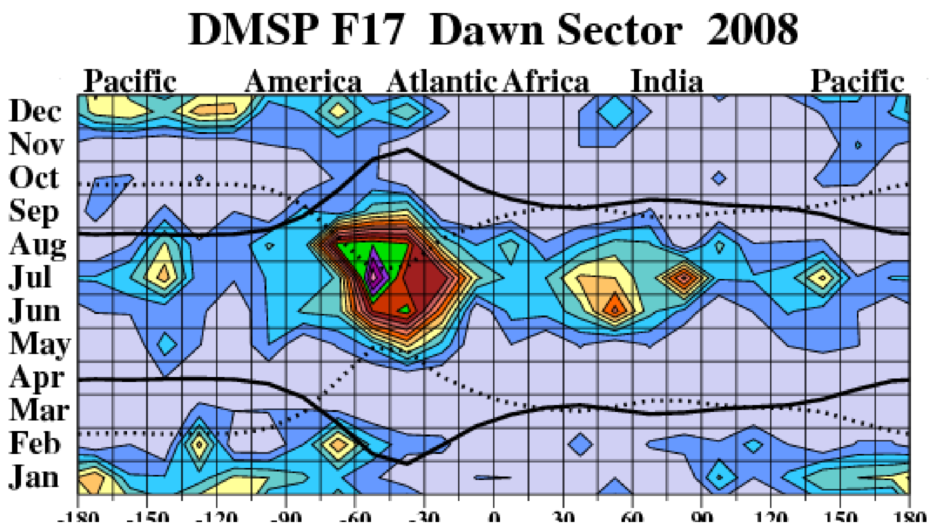

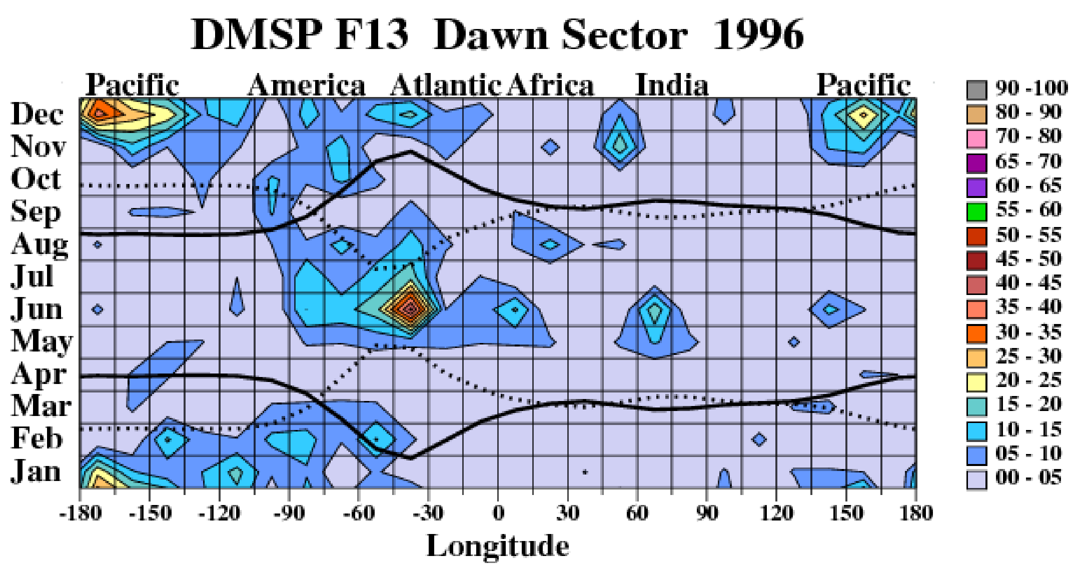

Equatorial Ionospheric Dynamics

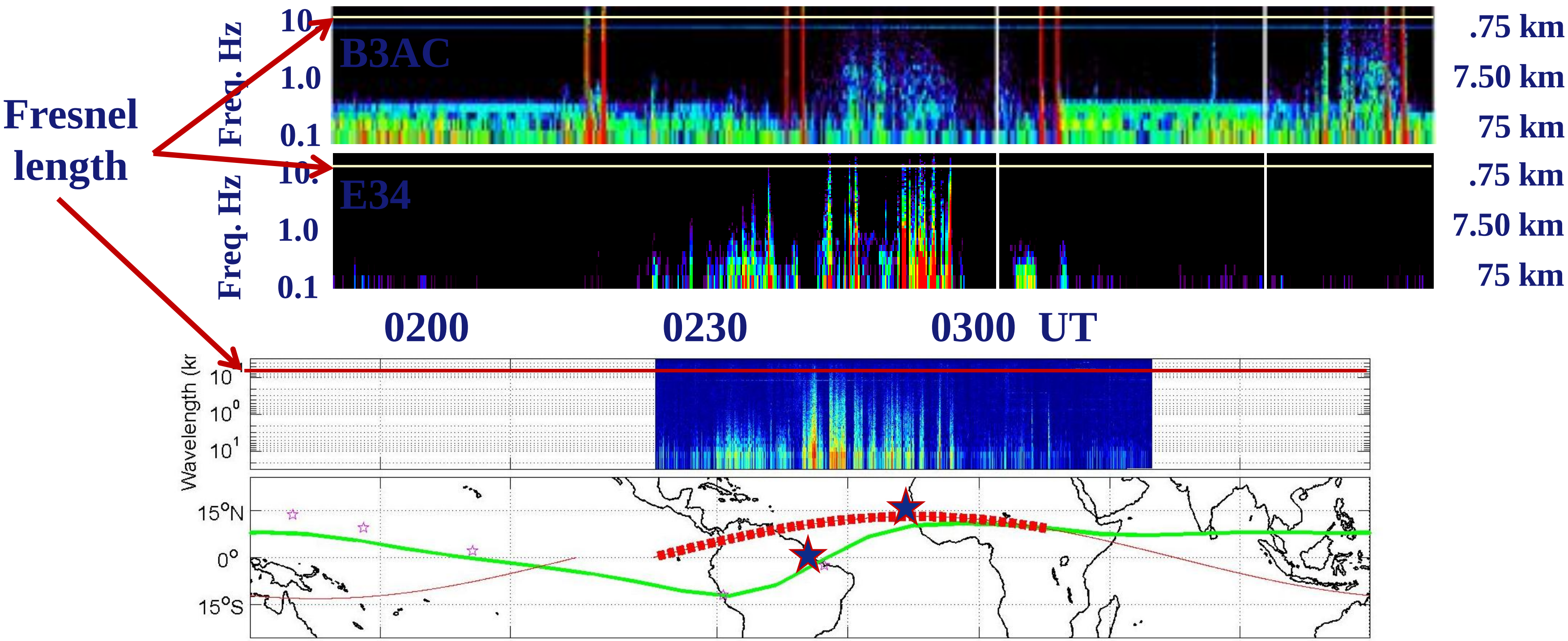

GLON	172.9	214.8	281.1	323.2	005.4	047.4	089.2	131.0
GLAT	-12.1	-05.1	+05.0	+12.1	+12.1	+05.2	-05.0	-12.1
GALT	752	588	443	404	481	639	792	838
MLON	246.4	286.1	351.2	040.5	077.5	118.8	159.7	202.3
MLAT	-16.5	-02.7	+16.8	+12.0	-01.2	-04.0	-15.5	-21.5
UT	03:37	03:49	02:24	02:36	02:47	02:59	03:12	03:24
SLT	15:00	18:00	21:00	00:00	03:00	06:00	09:00	12:00